remote sensing

MDPI

Article

Examination of Abiotic Drivers and Their Influence on *Spartina alterniflora* Biomass over a Twenty-Eight Year Period Using Landsat 5 TM Satellite Imagery of the Central Georgia Coast

John P. R. O'Donnell [1,*] and John F. Schalles [2]

[1] Department of Atmospheric Science, Creighton University, Omaha, NE 68178, USA
[2] Department of Biology, Creighton University, Omaha, NE 68178, USA; johnschalles@creighton.edu
* Correspondence: johnodonnell@creighton.edu; Tel.: +1-719-201-4920

Academic Editors: Deepak R. Mishra, Richard W. Gould Jr. and Prasad S. Thenkabail
Received: 12 April 2016; Accepted: 27 May 2016; Published: 4 June 2016

Abstract: We examined the influence of abiotic drivers on inter-annual and phenological patterns of aboveground biomass for Marsh Cordgrass, *Spartina alterniflora*, on the Central Georgia Coast. The linkages between drivers and plant response via soil edaphic factors are captured in our graphical conceptual model. We used geospatial techniques to scale up *in situ* measurements of aboveground *S. alterniflora* biomass to landscape level estimates using 294 Landsat 5 TM scenes acquired between 1984 and 2011. For each scene we extracted data from the same 63 sampling polygons, containing 1222 pixels covering about 1.1 million m^2. Using univariate and multiple regression tests, we compared Landsat derived biomass estimates for three *S. alterniflora* size classes against a suite of abiotic drivers. River discharge, total precipitation, minimum temperature, and mean sea level had positive relationships with and best explained biomass for all dates. Additional results, using seasonally binned data, indicated biomass was responsive to changing combinations of variables across the seasons. Our 28-year analysis revealed aboveground biomass declines of 33%, 35%, and 39% for *S. alterniflora* tall, medium, and short size classes, respectively. This decline correlated with drought frequency and severity trends and coincided with marsh die-backs events and increased snail herbivory in the second half of the study period.

Keywords: coastal remote sensing; salt marsh ecology; vegetation stress; ecosystem health; *Spartina alterniflora*; Landsat 5 TM; long-term data; climate forcing; river discharge; sea level

1. Introduction

Salt marshes are among the most productive natural ecosystems in the world [1,2] and provide numerous ecological services and economic benefits [3]. These important ecosystems are at risk from current and anticipated stressors, including sea level rise, higher average and peak temperatures, altered freshwater discharges and precipitation patterns, and more frequent droughts [4–8]. To date, climate induced changes have been associated with shifting vegetation phenologies, variations in biomass and/or net annual primary production (NAPP), and shifting species composition within marsh ecosystems [9–13]. Understanding how salt marsh ecosystems will continue to respond to a changing climate and additional anthropogenic disturbances are key questions for scientists, coastal reserve managers, conservationists, and coastal residents.

Vegetation indicators such as aboveground biomass and community composition are commonly used to evaluate overall health of coastal wetlands [14,15]. To understand the effects of climate-induced changes on ecosystem health and resilience, analysis of the influences abiotic drivers have on marsh productivity is required. However, traditional methods for monitoring plant biomass are field and

lab intensive, expensive, and normally constrained to one or several accessible local sites. Remote sensing with aerial and satellite sensor platforms provides an attractive alternative to estimate biomass and monitor ecosystem health at greater spatial and temporal scales [15,16]. Synoptic remote sensing methods can estimate canopy chlorophyll, green leaf area, aboveground biomass, and vegetation fraction at regional levels [17,18]. Remote estimations of these ecological indicators are possible using spectral reflectance transformations, referred to as vegetation indices (VIs) [14,19].

This study investigated the inter- and intra-annual dynamics of *Spartina alterniflora* biomass on the Central Georgia Coast (USA) and the influence of abiotic drivers on spatial and temporal biomass patterns during the operational period of Landsat 5 TM (1984–2011). In a recent study, Więski and Pennings [20] found that inter-annual differences in fall season *S. alterniflora* biomass on the Central Georgia Coast were best explained by Altamaha River discharge, sea level, and maximum summer temperature. Our primary objectives were to: (1) establish a data extraction and analysis scheme for identification of statistically significant relationships between biomass and abiotic drivers using Landsat data; (2) identify trends of *S. alterniflora* biomass throughout the 28-year study period and across each of three size classes; and (3) identify which climatic and other external variables best explained variations in *S. alterniflora* biomass across all seasons and with data binned by seasons. In this paper, we present an effective approach using Earth Observation Satellite (EOS) sensors for long-term observations of salt marsh response to changing climate patterns and efficient monitoring of salt marsh health.

2. Methods and Materials

2.1. Study Area

The Georgia coast occupies a 160 km stretch of southeastern North America, bordering the South Atlantic Bight (SAB) shelf system of the Western North Atlantic (Figure 1). The lower coastal plain of Georgia transitions to an extensive, interconnected network of coastal wetlands, salt marshes, river deltas, tidal rivers, and an outer chain of barrier islands fronting the Atlantic Ocean [21]. The Georgia coast is characterized by a sub-tropical climate with long, hot summers and brief, mild winters [22,23] (Figure 2). Rainfall concentrations are highest during the summer months, as a result of increased thunderstorms and occasional tropical storms (Figure 2).

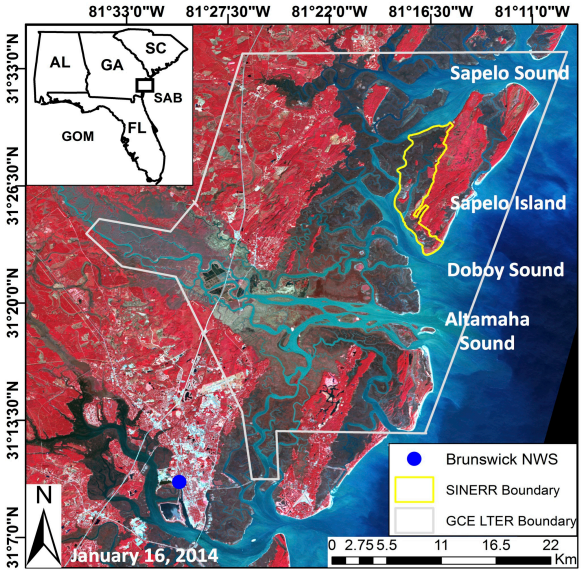

Figure 1. Landsat 5 color infrared image of the Brunswick National Weather Service (NWS) station, Sapelo Island National Estuarine Research Reserve (SINERR), and Georgia Coastal Ecosystems Long Term Ecological Research (GCE LTER) sites in Georgia.

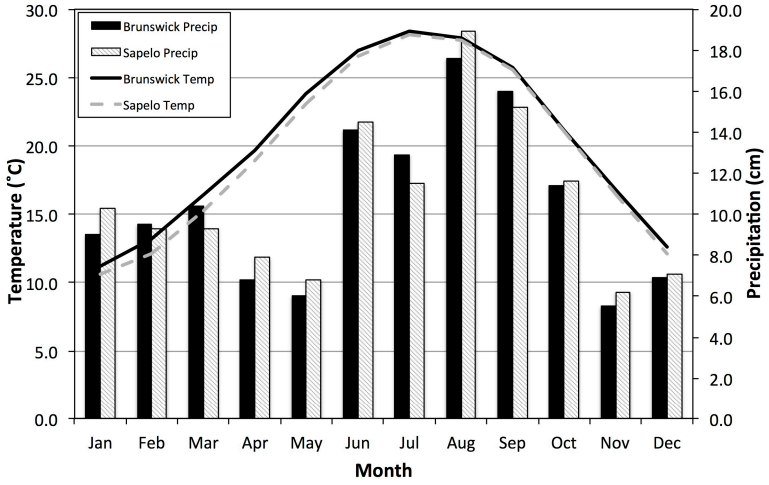

Figure 2. Monthly mean temperature and precipitation (1981–2010) for Brunswick and Sapelo Island, Georgia.

S. alterniflora is the dominate macrophyte in most salt marshes along the U.S. east coast, especially in Georgia. *S. alterniflora* occupies about 79% of the Duplin River marshes immediately behind Sapelo Island (Table 1). For this study, we used the Hladik *et al.* [24] height classification scheme for *S. alterniflora*: plants > 1 m were considered "tall" form; *S. alterniflora* < 0.5 m were "small" form; heights between 0.5 and 1 m were classified as "medium" form (Table 1). Along water channels, intertidal mud (10.0%) and tall-form *S. alterniflora* (16.2%) dominate the lowest elevations, transitioning to extensive medium-form (50.4%) and short-form *S. alterniflora* (12.3%) in mid to high marsh elevations. Other important marsh species occupy higher elevations, primarily between short-form *S. alterniflora* and the upland border (Table 1) [24]. Plant zonation patterns found along coastal Georgia, and within the Georgia Coastal Ecosystems (GCE) domain, are primarily driven by elevation gradients and water movement across the marsh platform [25].

Table 1. Summary of mean elevation (m) for each habitat class (species) measured in the Hladik and Alber [26] Real-Time Kinematic (RTK) survey within the Duplin River watershed, Georgia. Median biomass values and percent coverage of each habitat class are from the Schalles *et al.* [27] analysis of hyperspectral imagery acquired over the same watershed.

Species	RTK Elevation (m)	Biomass ($g \cdot dry \cdot wt \cdot m^{-2}$)	% Coverage
Tall *S. alterniflora*	0.36	1280.0	16.2
Medium *S. alterniflora*	0.77	695.0	50.4
Short *S. alterniflora*	0.87	325.0	12.3
All *S. alterniflora*	-	758.0	78.9
Intertidal Mud	0.89	0	10.0
S. virginica	0.95	890.0	3.8
D. spicata	0.96	-	-
B. maritima	0.99	1060.0	1.1
Salt Pan	1.01	0	1.4
J. roemerianus	1.02	1585.0	3.6
B. frutescens	1.23	1499.0	1.3

2.2. Landsat 5 TM Satellite Data

Landsat 5 Thematic Mapper (TM) data provided nearly continuous coverage of the earth's surface from 1984 to 2011 at a spatial resolution of 30 m. Given the across-track overlap of adjacent Landsat paths and rows (17/38 and 16/38), image acquisition covering our study site occurred twice every 16 days [28]. All multispectral Landsat 5 TM images were acquired from the United States Geological

Survey (USGS) Global Visualization Viewer (Glovis) website [29] and conformed to USGS Level 1T processing [30], which provides scene-to-scene registration with an error less than 7.3 m [31].

All Landsat images were filtered for tidal inundation effects (<0.65 m, relative to NAVD88) and cloud cover (<20% for entire LT 5 scene, plus cloud free study site). The 0.65 m criteria was established by comparing vegetation index behaviors at different tidal stages. Variations in tidal flooding of marshes significantly affects vegetation reflectance, especially in the near-infrared region, resulting in underestimation of aboveground biomass using vegetation index based algorithms [32]. Degree of tidal immersion was estimated using tide gauge data from Fort Pulaski, Georgia. Tide heights (relative to NAVD88) at the time of satellite acquisitions were compared against a tide gauge station (8677344) at nearby St. Simons Island, GA to determine offsets of the times of high and low tides. Data from St. Simons was only available for the period of 1999 to 2008. Our calculated offset (25 min) was then applied to Ft. Pulaski data to approximate tidal stage within the GCE domain at the time of image acquisition. These offset-corrected Ft. Pulaski values compare well to recent tidal heights (relative to NAVD88) recorded from the new GCE Carbon Flux Tower gauge, located on a small tributary just off the Duplin main channel. Using the above criteria, we selected 294 relatively cloud free scenes that provided coverage between March 1984 to November 2011. See O'Donnell and Schalles [33] for further details. Due primarily to seasonal variations in cloudiness, substantial differences existed in the number of useable scenes for each month, with a range of 9 (September) to 40 (April). All images were atmospherically corrected to surface reflectance using the Landsat Ecosystem Disturbance Adaptive Processing System (LEDAPS) software [34].

2.3. S. alterniflora Biomass Algorithm Development

Aboveground biomass data for *S. alterniflora* were collected concurrently with a hyperspectral flyover in June, 2006 [27]. *S. alterniflora* biomass values were obtained from harvesting all standing material (live and dead), at the soil line, in 0.25 × 0.25 m subplots. Harvested samples were sorted to live matter by species and dead matter, and these fractions were dried at 60 °C for 72 h (to constant weight) in ovens at the University of Georgia Marine Institute. A total of 161 *S. alterniflora* plots were collected along 14 transects covering low to high marsh zones. Four parallel AISA Eagle (63 bands, 1 m resolution) flight lines flown over the Duplin River tidal watershed on 20 June 2006 were individually georectified and atmospherically corrected, using Environment for Visualizing Images software (ENVI, Exelis VIS (Boulder, CO, USA)) Fast Line-of-sight Atmospheric Analysis of Hypercubes (FLAASH) and then combined as a mosaic using ENVI. For further details, see Schalles *et al.* [27] for plant sample processing and initial biomass mapping and Hladik *et al.* [24] for pre-processing of hyperspectral imagery and species-level mapping.

In order to accurately capture the relationship between field measurements and remote sensing data, a two-step approach was used to account for discrepancies between scaling up *in situ* clip-plot measurements to Landsat level pixels [35,36]. Model development began by comparing *in situ* clip-plot data for *S. alterniflora* plots against several vegetation indices derived from respective matched pixels in the AISA mosaic. Vegetation indices were calculated using reflectance values in the red (Band 30, 660 nm) and near-infrared (NIR) (Band 44, 799 nm) regions. Coefficient of determination (R^2) and overall fit of curve were used to determine model accuracy (Table 2). CI Red $((\rho NIR - \rho RED)/\rho RED)$ provided the best estimates for above ground *S. alterniflora* biomass ($R^2 = 0.70$). Prior to applying the biomass algorithm, non *S. alterniflora* pixels were masked using a hybrid multi-sensor (hyperspectral AISA Eagle and high resolution LIDAR) habitat classification map of the Duplin Watershed [24].

Table 2. The three best regression models for predicting *S. alterniflora* biomass using (A) AISA derived vegetation indices *versus in situ* clip plot biomass data and (B) Landsat 5 TM (LT 5) derived vegetation indices *versus* resampled (30 × 30 m) AISA biomass map. Note that R^2 values and adjusted R^2 values (not shown) were nearly identical. All regressions were calculated in JMP Pro 12 (SAS Institute, Inc. (Cary, NC, USA)).

Data Set	n	Index	R^2	Type	Equation	*p* value	F
(A) AISA	167	CI Red	0.70	Linear	$\text{Biomasss} = -212.36 + 952.47 \times \text{CI Red}$	<0.0001	386.4
	167	NDVI	0.70	Poly	$\text{Biomasss} = -829.17 + 4346.43 \times \text{NDVI} + 12070.72 \times (\text{NDVI} - 0.35)^2$	<0.0001	190.1
	167	$MSAVI_2$	0.66	Poly	$\text{Biomasss} = -1446.06 + 4273.76 \times MSAVI_2 + 10375.00 \times (MSAVI_2 - 0.49)^2$	<0.0001	159.8
(B) AISA *vs.* LT 5	1149	NDVI	0.51	Power	$\log(\text{Biomass}) = 9.86 + 3.22 \times \log(\text{NDVI})$	<0.0001	1195.2
	1149	$MSAVI_2$	0.51	Power	$\log(\text{Biomass}) = 9.31 + 4.29 \times \log(MSAVI_2)$	<0.0001	1205.2
	1149	CI Red	0.50	Power	$\log(\text{Biomass}) = 6.31 + 2.12 \times \log(\text{CI Red})$	<0.0001	1163.9

Concurrent with ground surveys and AISA hyperspectral flyover, a good quality multispectral Landsat 5 TM image was available from 28 June 2006 (Path 16/Row 38; 15:47:12 GMT; ~0.554 m tidal stage, relative to NAVD 88). To accurately scale up to Landsat level pixels, the AISA derived biomass map was resampled to 30 m^2 pixels using the nearest neighbor method in ENVI. Two "subscenes", as two polygon clusters totaling 1149 pixels (~1.34 million m^2), were selected from the resampled AISA biomass map to capture representative stands of each of the three *S. alterniflora* classes. Landsat derived vegetation indices of *S. alterniflora* pixels ($MSAVI_2$, EVI, NDVI, SAVI, WDRVI [37], CI Red [38], and TVI) were paired with the rescaled 30 m AISA biomass estimates from above. Vegetation indices were calculated using reflectance values from Landsat 5 TM Bands 3 and 4, covering the red and near-infrared (NIR) regions, respectively. Selection of an accurate and robust biomass algorithm from regressions was determined based on the coefficient of determination, the line of best fit, percent normalized root mean square error (% NRMSE) (Table 2), and user experience with summer biomass ranges. NDVI $((\rho NIR - \rho RED)/(\rho NIR + \rho RED))$ provided the best estimates for above ground *S. alterniflora* biomass (R^2 = 0.51) using the June 28 imagery data.

For model validation, a dataset was collected from areas of the resampled AISA biomass map not used for algorithm development. Forty pixels were randomly selected from each of the three size classes of *S. alterniflora* (n = 120). We then regressed these 120 predicted values (from the application of our NDVI algorithm to the entire June 28 Landsat scene) against "observed" AISA-derived biomass values in our resampled 30 × 30 m map. Recall that the AISA-derived map was calibrated with 161 clip-plot biomass field measures. In our model validation, a linear regression of observed *versus* predicted values yielded the equation:

$$\text{Observed biomass}\,(\text{g}\cdot\text{dry}\cdot\text{wt}\cdot\text{m}^{-2}) = 53.94 + (0.8229 \times \text{predicted biomass}) \quad (1)$$

with an R^2 of 0.763, F = 380.6149, p value < 0.0001, and RMSE = 296.1.

2.4. Pixel Selection for Consistent Extraction of Stand Samples by Size Class

A total of 63 sampling polygons were chosen for consistent sampling of Landsat data using the Environment for Visualizing Images (ENVI 5.1, Exelis VIS (Boulder, CO, USA)) Region of Interest (ROI) tool. Polygons were selected to accurately capture clusters of pixels specific to each of the three *S. alterniflora* size classes within our study site (Figure 3). To help ensure a consistent and accurate selection process and to account for possible variation in plant zonation over time, high resolution color infrared National Aerial Photography Program imagery, Google Earth Historical Imagery, and a high resolution vegetation classification map of the Duplin River watershed were used to delineate relatively homogenous stands. Contiguous pixels were then used to assemble polygons in each stand, with care taken to avoid mixed pixel effects caused by proximity to streams, upland borders, salt pans, and other marsh vegetation.

The 63 polygons were used to extract LEDAPS processed surface reflectance values from each of the 294 images. The polygons contained a total of 1222 pixels of *S. alterniflora* and covered about 1.1 million m^2 of Central Georgia salt marsh habitat (Table 3). Data extracted from each image were stored in a text file containing header information, x/y map coordinates, latitude/longitude coordinates, and band reflectance values for each pixel within a polygon cluster. These text files were imported into Microsoft Excel, where they were processed with two custom macros. The first macro calculated *S. alterniflora* aboveground biomass values for each pixel using the algorithm described above (Section 2.3). The second macro was then used to calculate average biomass values for each of the respective size classes and generate descriptive statistics for each scene.

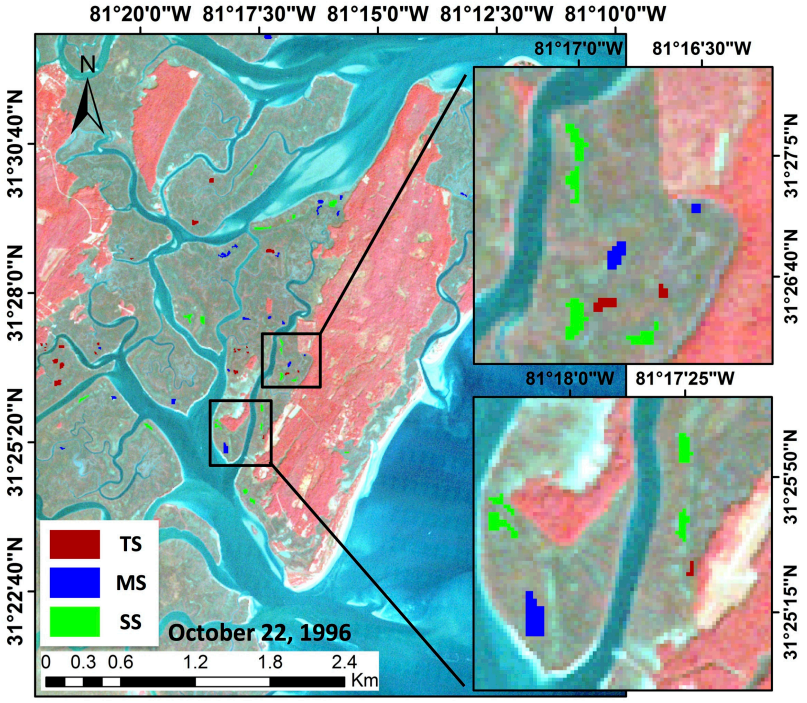

Figure 3. Landsat 5 color infrared image of Sapelo Island, GA and surrounding marshes highlighting polygon selection approach for extracting pixel clusters of different *S. alterniflora* size classes within our study site using Environment for Visualizing Images' (ENVI) Region of Interest (ROI) procedure.

Table 3. ENVI's Region of Interest (ROI) tool was used to extract polygons across the three height classes of *S. alterniflora*. The table depicts number of polygons, total pixels, and area covered by each of the three height classes of *S. alterniflora* sampled for this analysis.

Spartina Class	Polygons	Pixels	Area (m^2)
Tall (>100 cm)	24	312	280,800
Medium (50–100 cm)	20	368	331,200
Short (<50 cm)	19	542	487,800
Total	63	1222	1,099,800

2.5. Climate and Hydrology Data

Monthly mean climate and hydrology data for the 1984–2011 observation period, within proximity to our study site, were downloaded from publicly available sources (Figure 4; note abbreviations for each variable are shown in the key). Altamaha River discharge data were obtained from the U.S. Geological Survey (gage 02226000), near Doctortown, GA [39]. Mean sea level data (referenced to NAVD88) were taken from the National Oceanographic and Atmospheric Administration gages at Ft. Pulaski, GA (gage 8670870) and Fernandina Beach, FL (gage 8720030) [40]. Palmer Drought Severity Index (PDSI) and Standard Precipitation Index (SPI) data were taken from the National Climatic Data Center for the state of Georgia, Climate Division nine [41]. Note that negative, decreasing values of both PDSI and SPI correspond to deepening drought conditions.

Precipitation and air temperature data were taken from the National Weather Service (station 091340), near Brunswick, GA (Figure 4) [42]. A summary of monthly averaged values for all climate and hydrology data are presented in Figure A1 for the 28-year period of analysis.

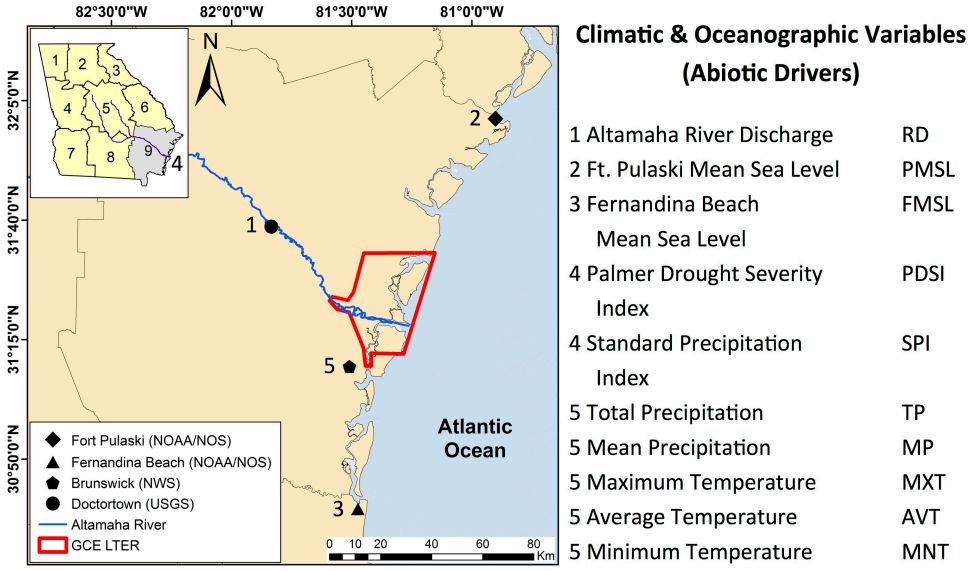

Figure 4. Map of Georgia Coast highlighting long-term monitoring stations and the ten abiotic drivers used in our study, along with abbreviations used in subsequent graphics.

2.6. Statistical Analyses

To identify the significance of each abiotic driver on *S. alterniflora* production, and to identify possible lagging effects for each variable, running means were calculated for three, six, and nine-month intervals prior to each image acquisition date. Monthly mean and running means were compared against mean values of biomass with simple linear regressions for each size class across all dates. A standard least squares procedure within the Fit Model platform of JMP Pro 12 (SAS Institute, Inc.) [43] was used in linear multiple regression models to examine the combined effects of multiple drivers on biomass. Collinearity among variables was determined through Pearson correlation matrices (Table A1) and Variance Inflation Factors (VIF). For this study, variables with VIF values above 2.5 (considered a conservative threshold) [44] were excluded from analysis.

To allow comparison of our remotely sensed biomass estimates with a previous Georgia Coastal Ecosystems 12-year study (2000–2011) of late growing season *S. alterniflora* biomass *versus* external drivers [20], we binned satellite observations for the same 12-year period and applied our linear univariate and multiple regressions procedures (noted as Fall 2000–2011). In addition, data for all years were binned into five periods to examine the influence of climate drivers across the annual growth and senescence cycles, using the following intervals: (1) the last week of September through the first week of November (simply noted as Fall); (2) within November and December; (3) within January and February; (4) within April and May; and (5) within July and August. Monthly mean and running mean values for drivers were analyzed, as above, with linear and multiple regressions.

3. Results

3.1. Overview of Biomass Findings

Mean biomass values for our 294 observations demonstrated good separation of the biomass classes with overall averages of 975.9, 580.7, and 373.8 g· dry· weight· m^{-2} for tall, medium, and short form. *S. alterniflora* biomass data were binned by acquisition month for all 28 years. Monthly averages depict seasonal phenology for each size class (Figure 5). Note the variation in the number of useable images for each of the twelve months. Our estimates compared favorably with the phenology patterns revealed with *in situ* clip-plot biomass measurements in previous studies within the Duplin River

marshes at Sapelo Island [45,46] and with monthly North Inlet, South Carolina biomass estimates measured from 1984 to 2011 [47].

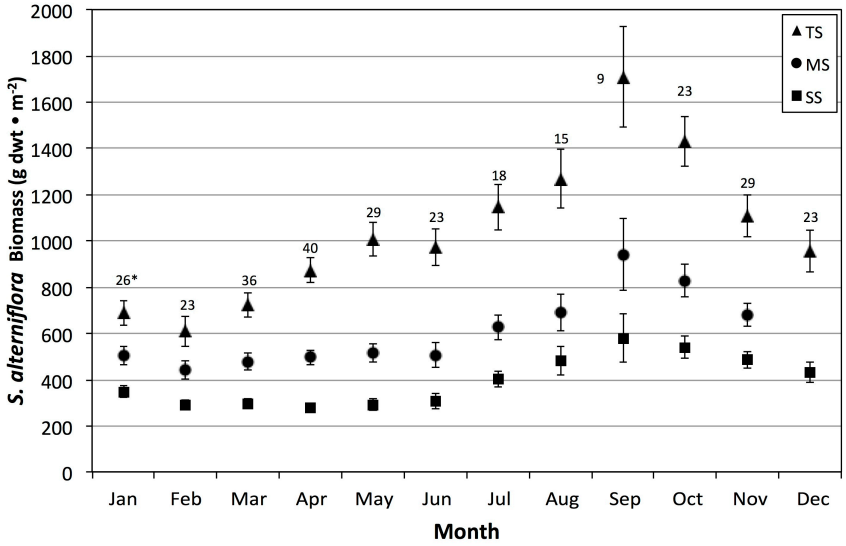

Figure 5. Mean monthly *S. alterniflora* biomass values for tall (TS), medium (MS), and short (SS) forms on the Central Georgia Coast. Data extracted from polygons across 294 Landsat 5 TM scenes; sorted by day-of-year, binned into month, and averaged for 28-year phenology patterns. * Number of images available for each month.

Minimum shoot biomass was observed in February. Tall form *S. alterniflora* stands at lower elevations and more favorable edaphic conditions had earlier and more robust spring growth (Figure 5). Small decreases in biomass were noted in June for both tall and medium *S. alterniflora* (Figure 5). This late spring dip in biomass accompanied a separately observed increase in shoot to root translocation of carbohydrates [48]. Peak biomass occurred in September, at a time of *S. alterniflora* flowering [49] followed by strong fall senescence of shoot biomass and corresponding translocation to roots (Figure 5).

In order to display and examine temporal variation in *S. alterniflora* biomass, values for each of the three height classes from the 294 images were plotted for the 28-year observation period (Figure 6). We found strong, but highly variable seasonality and inter-annual growth and senescence patterns. Consistent separation of biomass levels for the three height classes indicate these community patterns can persist for relatively long periods of time. Furthermore, our pixel selection procedure accurately captured spatial heterogeneity along the marsh elevation gradient that controls *S. alterniflora* growth patterns. Biomass values were suppressed in drier periods (e.g., 2002–2003) and were generally highest in wet and/or cooler summers (e.g., 1995–1997). Even a single year of higher moisture (1987) resulted in high biomass, followed by low biomass in 1988 (Figure 6). An extreme hard freeze during January, 1985 was followed by reduced late winter and spring biomass.

Over the 28-year period, *S. alterniflora* biomass had a significant overall decline, suggesting decreased marsh health (Figure 6). This observation appears related to increased drought and reduced river discharge during the second half of our 28-year period of record. Regression analysis of our Landsat-derived aboveground biomass estimates showed size class declines over our 28-year observation period of 393, 250, and 185 g· dry· weight· m^{-2}; representing 33%, 35%, and 39% reductions for tall, medium, and short, respectively (Table 4). These calculations were interpolated by applying the starting and ending dates of our observational period to the regression equation (Figure 6). Although high intra and inter-annual variations resulted in high RMSE and low R^2 values for each size class, probability ($p < 0.0001$) and F value estimates for these regression equations were highly significant (Table 4). We interpolated our 28-year monthly binned data to produce day-of-year look up tables

(see gray lines in Figure 6), allowing calculation of deviations of biomass for each observation date and size class. This analysis largely removed the effect of the average phenological patterns from our data. The resulting equations (Table 5) yielded biomass change values close to those in Table 4 and strongly supported the conclusion of serious declines in above ground biomass, with percentage reductions of 32%, 34%, and 39% for tall, medium, and short, and moderate improvements in the R^2 and F values (Table 5). Most of the residual "error" in this later analysis is associated with intra and inter-annual variations due to abiotic drivers and biotic interactions.

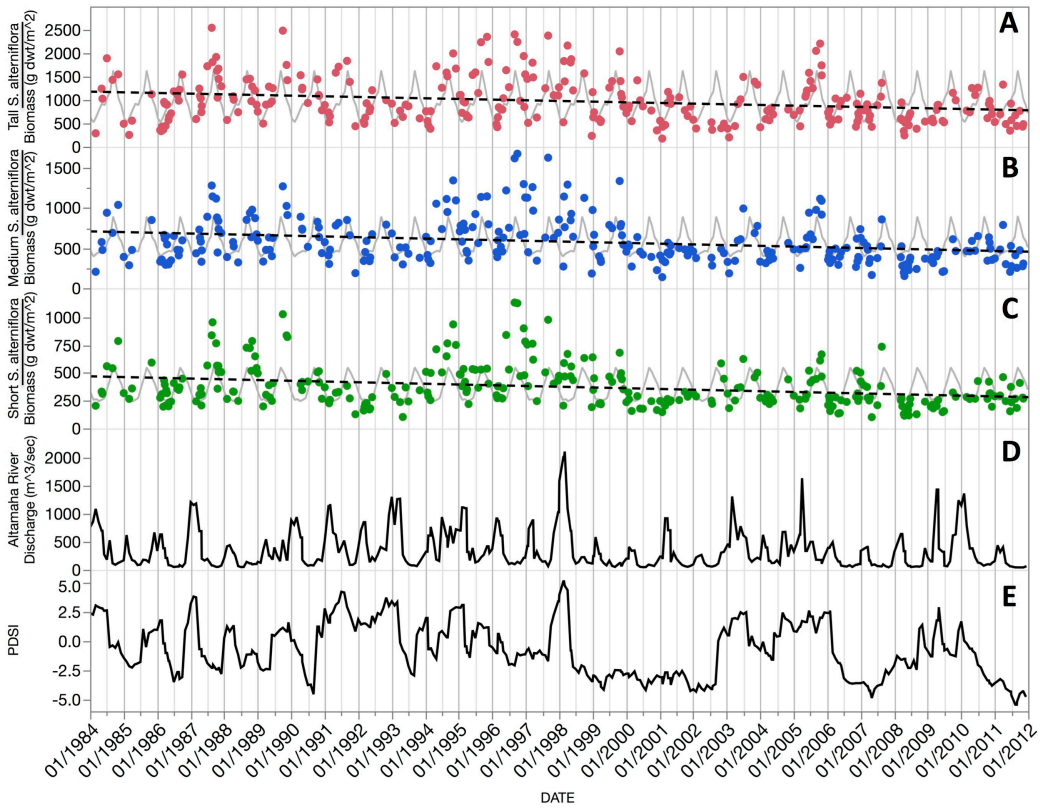

Figure 6. Extracted biomass values from Landsat 5 data for three height classes of *S. alterniflora* (**A**) tall; (**B**) medium; and (**C**) short size classes over the 28 year study period. Gray line corresponds to day-of-year look up table values calculated by interpolation of the binned monthly biomass estimates in Figure 5. Regression equations and coefficient of determination for (**A**) y = 2373.84 − 0.0389x; 0.057; (**B**) y = 1469.35 − 0.0247x; 0.067; and (**C**) y = 1030.64 − 0.0183x; 0.081. Also shown are mean monthly values for (**D**) Altamaha River Discharge at Doctortown, GA and (**E**) Palmer Drought Severity Index for region 9 in Georgia (Figure 4).

Table 4. Results of fitting a simple linear regression line for the 28-year period of observation for biomass estimates of the three size classes of *S. alterniflora* (n = 294; see Figure 6).

	Tall ($g \cdot dry \cdot wt \cdot m^{-2}$)	**Medium** ($g \cdot dry \cdot wt \cdot m^{-2}$)	**Short** ($g \cdot dry \cdot wt \cdot m^{-2}$)			
March 1984	1177.1	708.2	468.5			
November 2011	783.9	458.2	283.8			
Estimated Decline	393.2	249.9	184.8			
% Change	33.3	35.2	39.3			
***Spartina* Class**	**a**	**B**	**R^2**	***p* value**	**F**	**RMSE**
Tall	2373.8	−0.03892	0.0571	<0.0001	17.70	463.9
Medium	1469.4	−0.02474	0.0667	<0.0001	20.87	271.5
Short	1030.6	−0.01829	0.0811	<0.0001	25.75	180.7

Table 5. Results using deviations from annual phenology calculated from day-of-year values for each image.

	Tall ($g \cdot dry \cdot wt \cdot m^{-2}$)	Medium ($g \cdot dry \cdot wt \cdot m^{-2}$)	Short ($g \cdot dry \cdot wt \cdot m^{-2}$)			
March 1984	191.5	121.1	92.8			
November 2011	−182.1	−117.0	−89.4			
Estimated Decline	373.6	238.0	182.2			
% Change	31.7	33.6	38.9			
***Spartina* Class**	**a**	**B**	**R^2**	***p* value**	**F**	**RMSE**
Tall	1328.9	−0.03698	0.0735	<0.0001	23.16	385.4
Medium	845.6	−0.02356	0.0755	<0.0001	23.85	242.0
Short	647.3	−0.01803	0.1064	<0.0001	34.76	153.4

3.2. Analysis of Variation across 28 Years and All Dates

Across all dates, univariate analysis identified minimum temperature as the best predictor (positive influence) for *S. alterniflora* biomass (Table A2). Current month minimum temperature best predicted tall, whereas six month minimum temperature best predicted medium and short form biomass. The best models from multiple regression analysis used river discharge, total precipitation, and minimum temperature and (for short form) Fort Pulaski mean sea level (Table 6 and Figure 7). Each variable had a positive influence. The multivariate models had R^2 values of 0.408, 0.326, and 0.351 for tall, medium, and short forms.

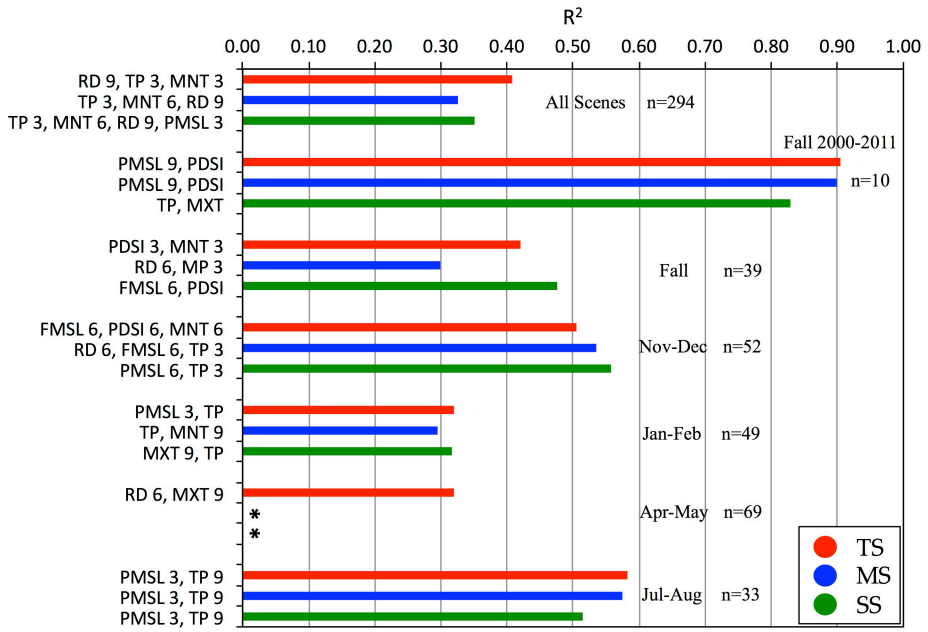

Figure 7. Multivariate analysis results for tall (TS), medium (MS), and short (SS) *S. alterniflora versus* abiotic drivers across each of the seven-binned periods. Driver abbreviations: Altamaha River Discharge (RD), Ft. Pulaski Mean Sea Level (PMSL), Fernandina Beach Mean Sea Level (FMSL), Palmer Drought Severity Index (PDSI), Total and Mean Precipitation (TP and MP), and Maximum and Minimum Temperature (MXT and MNT). * Unable to identify best multivariate model due to collinearity among variables.

Table 6. Best univariate and multivariate regression model abiotic drivers for predicting *S. alterniflora* biomass for each size class, Tall (TS), Medium (MS), and Short (SS): (A) all dates (n = 294) from 1984 to 2011, (B) between the last week of September through the first week of November (n = 10) from 2000 to 2011; (C) between the last week of September through the first week of November (n = 39) from 1984 to 2011; (D) within November and December (n = 52), (E) within January and February (n = 49), (F) within April and May (n = 69), and (G) within July and August (n = 33). Note that all single and multivariate analyses were positive relationships and the four bimonthly-binned periods used the entire 1984–2011 observation period.

Date	Class	Best Predictor	R^2	Multivariate Analysis	R^2	Adjusted R^2	p	VIF 1	VIF 2	VIF 3	VIF 4
(A) All Dates	TS	MNT 3	0.271	RD 9, TP 3, MNT 3	0.408	0.402	<0.0001	1.05	1.24	1.21	
	MS	MNT 6	0.173	TP 3, MNT 6, RD 9	0.326	0.319	<0.0001	1.23	1.18	1.08	
	SS	MNT 6	0.247	TP 3, MNT 6, RD 9, PMSL 3	0.351	0.342	<0.0001	1.26	2.49	1.10	2.45
(B) Fall 2000–2011	TS	FMSL 9	0.874	PMSL 9, PDSI	0.905	0.877	0.0003	2.33	2.33		
	MS	FMSL 9	0.840	PMSL 9, PDSI	0.899	0.871	0.0003	2.33	2.33		
	SS	PMSL 9	0.766	TP, MXT	0.829	0.780	0.0021	1.25	1.25		
(C) Fall	TS	PDSI 3	0.324	PDSI 3, MNT 3	0.420	0.388	<0.0001	1.00	1.00		
	MS	PDSI	0.241	RD 6, MP 3	0.299	0.260	0.0017	1.16	1.16		
	SS	MP 3	0.212	FMSL 6, PDSI	0.476	0.447	<0.0001	1.04	1.04		
(D) Novembe–December	TS	MP 3	0.314	FMSL 6, PDSI 6, MNT 6	0.505	0.474	<0.0001	1.04	1.01	1.04	
	MS	TP 3	0.379	RD 6, FMSL 6, TP 3	0.535	0.506	<0.0001	1.69	1.07	1.66	
	SS	TP 3	0.371	PMSL 6, TP 3	0.558	0.540	<0.0001	1.00	1.00		
(E) Januar–February	TS	PMSL 3	0.256	PMSL 3, TP	0.320	0.290	0.0001	1.03	1.03		
	MS	PMSL 3	0.242	TP, MNT 9	0.295	0.264	0.0003	1.01	1.01		
	SS	MXT9	0.261	MXT 9, TP	0.317	0.287	0.0002	1.00	1.00		
(F) Apri–May	TS	RD 6	0.284	RD 6, MXT 9	0.320	0.299	<0.0001	1.04	1.04		
	MS	RD 3	0.292	* Unable to identify multivariate model due to collinearity among variables.							
	SS	RD 6	0.180	* Unable to identify multivariate model due to collinearity among variables.							
(G) July–August	TS	SPI 9	0.535	PMSL 3, TP 9	0.582	0.555	<0.0001	1.00	1.00		
	MS	SPI 9	0.452	PMSL 3, TP 9	0.575	0.546	<0.0001	1.00	1.00		
	SS	SPI 9	0.349	PMSL 3, TP 9	0.515	0.482	<0.0001	1.00	1.00		

3.3. Analysis of Seasonal Biomass Variation Using Binned Data

Nine month Fort Pulaski Mean Sea Level and current month Palmer Drought Severity Index were our best combined predictors for the fall 2000–2011 analysis period (Table 6), with positive influences for tall and medium forms. However, short form was best predicted using current month total precipitation (positive influence) and current month maximum temperature (negative influence). This 12-year period, which had the greatest overall driver variability within our study period, also accounted for the highest R^2 values of all our analyses (0.905, 0.899, and 0.829, for tall, medium, and short forms; Figure 7).

In our expanded, 28-year Fall period analysis (last week of September through the first week of November, n = 39; Table 6) average biomass values and ranges for single dates in this period were 1382 (386–2485 for tall), 825 (241–1678 for medium), and 553 (128–1132 for short) g dry weight · m^{-2}. Compared to the 12-year analysis above, regression results were less robust and best predictor variables were often different (Table 6, Figure 7, and Table A2). In multiple regression analysis, different combinations of variables (precipitation, discharge, sea level, minimum temperature and Palmer Drought Severity Index, all positive influences) were best predictors of the three size classes (Table 6 and Figure 7).

In addition to external drivers, we examined the effect of the previous year's Fall biomass condition on current year Fall biomass. Based on linear regression R^2, biomass in the previous fall period accounted for 23%, 31%, and 15% of variability in the subsequent Fall period for tall, medium, and short *S. alterniflora*, respectively. When this variable was included in the multiple regression analysis for our 28-year Fall analysis, R^2 values improved from 0.420 to 0.525, 0.299 to 0.455, and 0.476 to 0.546 for tall, medium, and short forms. Presumably this effect demonstrates that the degree of replenishment of root tissues during fall translocation plays an important role in spring translocation to shoots and resultant growing season net primary production (NPP).

In our November-December period, aboveground biomass is rapidly decreasing. Three month integrated precipitation (mean and total precipitation) were the best univariate predictors for this period (Table A2). Combinations of six month sea level, six month river discharge, six month Palmer Drought Severity Index, and three month total precipitation accounted for half or more of the biomass variations in this period (Table 6 and Figure 7). Our data indicate moisture availability and salinity still exert strong influence, even though solar insolation, temperatures, and primary production rates rapidly decrease in this period.

January-February biomass was best explained in multivariate regressions using combinations of current month total precipitation, three month sea level (Fort Pulaski gauge) and nine month temperatures (Table 6 and Figure 7). Thus, the magnitude of marsh flooding, precipitation and temperatures were positively related to, and best predicted winter biomass.

For the mid-spring period (April–May), multiple regression analysis determined that six month river discharge and nine month maximum temperature were the best combination to explain tall form variation. However, because of collinearity, no combinations of variables could be identified for medium and short form. In univariate analysis, river discharge, Palmer Drought Severity Index, and precipitation best accounted for April-May biomass variation (Table A2). Finally, for mid-summer (July-August), multivariate regressions identified the combination of three month Fort Pulaski Mean Sea Level and nine month total precipitation as the best, and strong predictors of biomass for all three classes (Table 6, Figure 7). It is notable that simple and multiple regression R^2 values were much higher for the July-August period than the April-May period (Table 6 and Figure 7). This outcome is likely the result of higher inter-annual variability in mid-summer biomass. Vegetation stress is likely to be greatest when both temperature and soil salinity peak, especially during drought conditions.

4. Discussion

This study demonstrated the utility of using long-term Thematic Mapper optical data from a single NASA Earth Observation Satellite (EOS) mission, Landsat 5, that provided the longest continuous

record of any EOS. We developed a scheme to: (1) scale-up ground truth clip-plot *S. alterniflora* aboveground biomass from our study area to match the 30 m resolution of Landsat 5; (2) create and extract polygons from 28 years of imagery that represented clusters of three operational size classes occurring across the marsh elevation gradient and covered ~1.1 million m^2 of Central Georgia salt marsh; and (3) combine long-term biomass observations with climate, hydrology, and meteorological data to account for short to longer duration vegetation behavior.

We established that *S. alterniflora* production in Southeastern U.S. subtropical marshes is responsive at any time of year to abiotic drivers. For example, overwintering aboveground biomass is variable and appears most vulnerable to moisture stress from reduced precipitation and lower sea level. The duration of stress is important. Three, six, and nine month periods prior to image acquisitions all emerged as significant at certain times of year and with one or more size classes (Figure 7). Not surprisingly, our best regression results (Figure 7) matched the periods of greatest biomass change (notably mid-summer and mid-fall, see Figure 5) or the longer durations and greater deviations from average phenology biomass (day-of-year gray line in Figure 6) that occurred in the second half of our study (1998–2011).

Overall, temperature accounted for the greatest amount of temporal variability, primarily as a positive influence on the phenology of net primary production. However, the entire suite of variables determine the degree to which biomass deviates according to stress-subsidy responses [50] from the average phenology (Figure 6). In the winter, higher sea level, precipitation, and temperature promote higher biomass (Figure 7). Increased river discharges and precipitation in winter lead to higher spring biomass. By mid-summer, however, higher sea level and/or total precipitation account for higher biomass whereas drought and high temperature stress result in lower than average biomass. By mid-fall to early winter, vegetation biomass responds most strongly to higher sea level, precipitation, and temperatures.

S. alterniflora physiology and productivity are directly driven by the physical and chemical properties within salt marsh sediments. Overall, soil salinities and other stressors in marshes (Figure 8) are determined by the salinity of ambient tidal water, the frequency of tidal flooding along marsh elevation gradients, recent precipitation on the marsh, and solar radiation as a driver of evapotranspiration and soil hypersalinization [51,52]. These effects vary across the *S. alterniflora* elevation stress gradient. Plant stress can also lead to stronger herbivory and top-down controls on marsh plants [53].

Precipitation in any season directly dilutes salt that accumulates in soils and provides moisture (Figure 8). For example, increased precipitation was associated with higher biomass in July and August, but also in our coldest two periods (November-December and January-February, Figure 7). These results are consistent with previous findings by Dame and Kenny [54], Gross *et al.* [55], and Więski and Pennings [20].

High Altamaha River discharges decrease the salinities of interconnected nearshore channels and the inner shelf waters [56] and increase nitrogen and phosphorous supplies [57]. When coupled with higher sea levels, tidal flushing lowers porewater salinities, increases dissolved oxygen and limiting nutrients, and removes excess wastes (metabolites) and detritus (Figure 8) [52].

Both our study and Więski and Pennings [20] found strong intra-annual differences in drivers and biomass responses for early fall during a common period of study (2000–2011). Biomass ranges were comparable, even though Więski and Pennings used non-destructive, site-specific allometric equations from fewer and smaller sampling areas *versus* our more synoptic remote sensing procedure. Both studies established that Altamaha River discharge, sea level, temperature, and precipitation had positive correlations with and were generally the best predictors of mid-fall biomass and that maximum temperature had a negative correlation with late growing season biomass. Also, in both studies, higher sea levels (Fort Pulaski and, or Fernandina gauges) were associated with increased aboveground biomass for all three size classes along the marsh elevation gradient. Several studies have shown an increase in *S. alterniflora* biomass productivity with increasing water levels at mid-marsh

elevations [58]. In our period of our study, sea level variations were more affected by meteorology (changes in the direction and force of winds) [56] than the slow, additive rates of sea level rise.

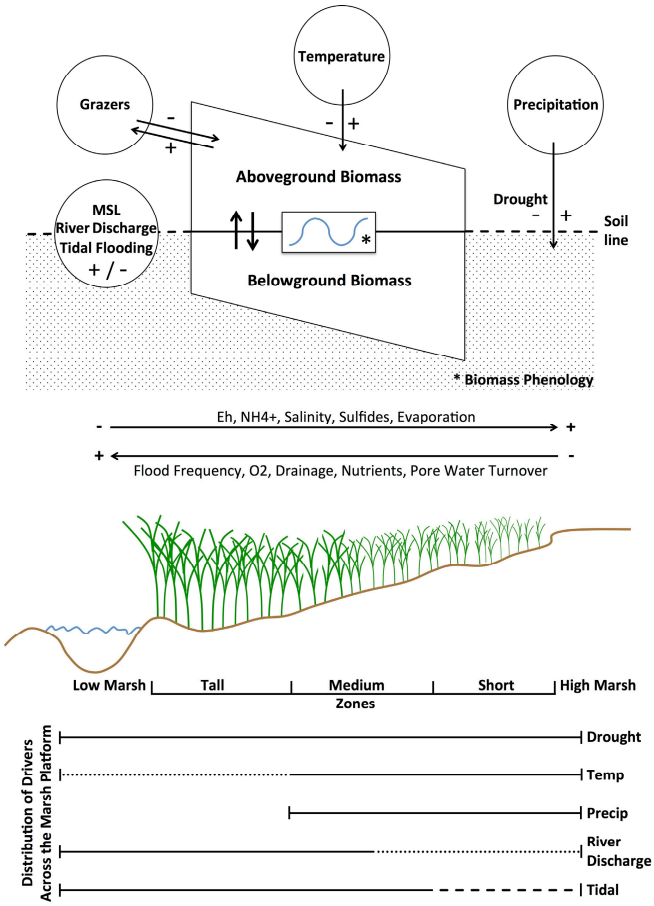

Figure 8. Conceptual model linking abiotic drivers to aboveground biomass via soil mediated interactions within the elevation gradient of the marsh platform. Gradient arrows (center) adapted from Mendelssohn and Morris [52].

Unlike Więski and Penning's study, we were also able to examine the influence of abiotic drivers on other periods of the year. In the subtropical climate of the Central Georgia Coast, primary production and net growth are possible at any time of the year, although the period between October and February had overall declines in average monthly aboveground biomass (Figure 5). To increase sample sizes but avoid strong inter-monthly variation, we selected four bimonthly binned periods to examine the effects of abiotic variables at different phenology stages across our 28-year study period.

Consistent with our temperature response data, carbon fixation and net photosynthesis increased in all seasons in *S. alterniflora* with modest temperature increases [59]. Conversely, temperature stress was linked to decreased biomass during periods of drought and above average summer temperatures. During summer chamber experiments in Sapelo Island marshes, Giurgevich and Dunn [59] found that net photosynthesis rates peaked at about 30–32 °C for both short and tall form *S. alterniflora*. They measured significant reductions in net photosynthesis, leaf diffusive conductance to water vapor, and water use efficiencies between 35 and 45 °C. With anticipated increases in summer maximum temperatures [60], *S. alterniflora* may become more constrained by reduced periods of optimal temperatures and decreased NPP and through stress induced by a combination of higher temperatures and soil salinities and by lower soil redox potential (Eh).

Recent, prolonged droughts were associated with small to large-scale die-back events of *S. alterniflora* [61]. The direct causes of dieback events are complex, but both abiotic and biotic

stressors have been identified as contributing factors [62]. Droughts have profound impacts on the interactions between marsh plants, grazers, and fungi. For example, during extended periods of drought *Littoraria irrorata* snails exert strong negative effects on short form *S. alterniflora* biomass [63]; however, these effects can extend into healthier stands at lower elevations [53]. Fungi in the genus *Fusarium* directly damaged *S. alterniflora* under high salt stress and made plants more susceptible to purple marsh crab (*Sesarma reticulatum*) and root nematode herbivory [61]. The recurrent, highly reduced biomass between 2000 and 2011 (Figure 6) may thus be explained by a combination of drought induced plant stress combined with snail, crab, and *Fusarium* damage. Salt marsh biomass declines and diebacks could be similar to recent, widespread forest declines [64], where drought intensification leads to negative plant carbon balance, increased vulnerability to herbivores (bark beetles), and, when prolonged, tree death spirals.

The extended periods of drought and related maximum summer temperature regimes since 2000 help to explain the net *S. alterniflora* biomass decline over our 28-year study (Table 4). Whether this decline is a portent of longer-term declines is unknown. Challenges to this keystone species and marsh ecosystem health are being addressed by the Georgia Coastal Ecosystems LTER long-term research program and the development of a comprehensive, linked set of models to portray plant ecophysiology and gross and primary production in a spatially explicit manner. Our remote sensing approach can play an important role in addressing this question not only on the Central Georgia Coast, but in many other coastal locations.

5. Conclusions

The ability to remotely differentiate size classes and thus analyze biomass responses along the marsh platform's elevation gradient affords insights of *S. alterniflora's* adaptations to resources and stressors (Figure 8). Our study identified river discharge, mean sea level, temperature, precipitation, drought, and previous year's biomass as important predictors of *S. alterniflora* production. Although most evident in seasonal or inter-annual periods of accelerated biomass change, the drivers we studied exert affects throughout the year and their magnitudes largely determine deviations from average biomass phenology.

Our 28-year record of aboveground biomass revealed a serious and recent decline in the emergent macrophyte, *S. alterniflora*, in Coastal Georgia. It seems likely that this aggregate response is largely drought driven and the result of reduced flushing of marsh soils and warmer temperatures, leading to reduced nutrient loading, increased salinities, more extensive anaerobic conditions with elevated sulfide and ammonia levels, and greater herbivore damage (Figure 8). Declines at lower elevations may also be related to variations in sea levels and accelerated physical and biological erosion along river and creekbanks and the margins of more isolated intertidal mudflats [65].

This study has demonstrated the value of using remote sensing techniques and Earth Observing Satellites to monitor seasonal and long-term patterns of primary production as opposed to studies primarily based on end-of-season biomass (NAPP). The ability to accurately monitor and capture phenological trends can assist modeling efforts to better understand the interactions of environmental controls on vegetation across all seasons. However, in coastal habitats, selection of imagery requires careful assessment of tidal inundation as well as proper atmospheric corrections and georectification. This sampling method can accurately reveal large-scale patterns, making it easier to extrapolate hypotheses and conclusions to the ecosystem and landscape levels, as opposed to reliance on plot-based measurements. Finally, this study established a methodological approach that can be continued at our site and carried to other sites or regions, allowing scientists and reserve managers to better examine the influence of climatic and other external drivers via bottom-up and top-down controls on primary production within salt marsh ecosystems.

Acknowledgments: This project was funded by the National Science Foundation, Georgia Coastal Ecosystems Long Term Ecological Research award (OCE-12237140) and the National Oceanic and Atmospheric Administration, Office of Education Educational Partnership Program award (NA11SEC4810001). The contents of this publication

are solely the responsibility of the award recipient and do not necessarily represent the official views of *the U.S. Department of Commerce, National Oceanic and Atmospheric Administration*. We wish to thank Steve Pennings and Kazimierz Więski for their guidance, advice, and patience throughout this study; Deepak Mishra for assistance with biomass algorithm development; Merryl Alber and Wade Sheldon for climate index data sets; and Alistair Cullum and James Ault for assistance with statistical analyses. This work greatly benefitted from discussions with Kevin Gallo, Mackenzie Taylor, and Tim Wagner, who served as members of John O'Donnell's thesis committee. We would like to thank Steve Pennings and four anonymous reviewers for their helpful comments on the manuscript. Landsat Surface Reflectance data products were courtesy of the U.S. Geological Survey Earth Resources Observation and Science Center. This is Contribution Number 1047 of the University of Georgia Marine Institute. This work is a contribution of the Georgia Coastal Ecosystems Long Term Ecological Research project. Finally, we thank the Graduate School at Creighton University for support of this publication and the staff of the Sapelo Island National Estuarine Research Reserve for their encouragement and support of this study.

Author Contributions: Both authors contributed to writing the text, editing, and reviewing the manuscript.

Conflicts of Interest: The authors declare no conflict of interest.

Abbreviations

NAPP	Net Annual Primary Production
RD	River Discharge
PMSL	Fort Pulaski Mean Sea Level
FMSL	Fernandina Beach Mean Sea Level
MP	Mean Precipitation
TP	Total Precipitation
PDSI	Palmer Drought Severity Index
SPI	Standard Precipitation Index
MXT	Maximum Temperature
AVT	Average Temperature
MNT	Minimum Temperature
EOS	Earth Observing Satellite

Appendix

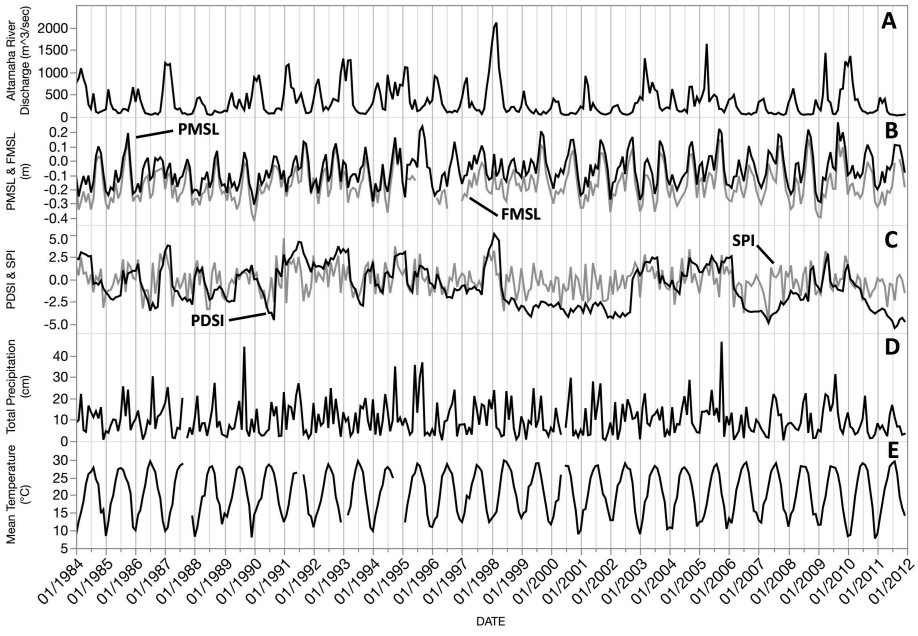

Figure A1. Monthly mean values for (**A**) Altamaha River Discharge at Doctortown, GA; (**B**) Mean Sea Level relative to NAVD88 for Fort Pulaski, GA and Fernandina Beach, FL; (**C**) Palmer Drought Severity Index (PDSI) and Standard Precipitation Index (SPI) for Georgia, region nine; (**D**) Total Precipitation and (**E**) Mean Temperature at Brunswick, GA over a 28-year period. Note that SPI was multiplied by 1.5 in order to amplify the signal to better identify trends when plotted. Gaps in data represent periods of missing observations.

Table A1. Pearson's correlation coefficients (lower matrix) and probability values (upper matrix) for external drivers and biomass of three *S. alterniflora* height classes across all dates (n = 294) from 1984 to 2011. The correlations are estimated by the Pairwise method.

	Mean TS Biomass	**Mean MS Biomass**	**Mean SS Biomass**	**RD**	**PMSL**	**FMSL**	**PDSI**	**SPI**	**TP**	**MP**	**MXT**	**AVT**	**MNT**
Mean TS Biomass		<0.0001	<0.0001	0.5593	<0.0001	<0.0001	0.0006	0.0587	0.0001	0.0002	<0.0001	<0.0001	<0.0001
Mean MS Biomass	0.920		<0.0001	0.7798	<0.0001	<0.0001	0.0002	0.0051	0.0005	0.0006	0.0271	0.0057	0.0012
Mean SS Biomass	0.794	0.921		0.294	0.0003	<0.0001	0.0187	0.0025	0.0012	0.0015	0.1972	0.0775	0.0291
RD	−0.036	0.017	−0.064		<0.0001	0.0023	<0.0001	<0.0001	0.0219	0.0115	<0.0001	<0.0001	<0.0001
PMSL	0.374	0.279	0.218	−0.246		<0.0001	0.3721	0.3379	0.0009	0.0011	<0.0001	<0.0001	<0.0001
FMSL	0.347	0.289	0.251	−0.186	0.959		0.5787	0.391	0.1112	0.1157	0.0004	<0.0001	<0.0001
PDSI	0.209	0.226	0.144	0.597	−0.055	0.034		<0.0001	<0.0001	<0.0001	0.0015	0.0075	0.0286
SPI	0.116	0.171	0.184	0.319	0.059	0.053	0.551		<0.0001	<0.0001	0.0017	0.0218	0.1306
TP	0.231	0.211	0.197	0.140	0.202	0.098	0.331	0.688		<0.0001	0.0077	0.0005	<0.0001
MP	0.227	0.208	0.193	0.154	0.199	0.096	0.342	0.692	0.999		0.0104	0.0008	<0.0001
MXT	0.320	0.135	0.079	−0.303	0.374	0.214	−0.193	−0.191	0.163	0.156		<.0001	<.0001
AVT	0.353	0.169	0.108	−0.290	0.409	0.251	−0.163	−0.140	0.211	0.204	0.993		<.0001
MNT	0.379	0.197	0.133	−0.274	0.436	0.282	−0.134	−0.093	0.252	0.245	0.974	0.994	

Table A2. Top three abiotic drivers best predicting *S. alterniflora* biomass across each height class for (A) all dates (n = 294) from 1984 to 2011, (B) all dates falling between the last week of September through the first week of November (n = 10) from 2000 to 2011; and all dates 1984–2011 (C) within the last week of September through the first week of November (n = 39), (D) within November and December (n = 52), (E) with in January and February (n = 49), (F) within April and May (n = 69), and (F) within July and August (n = 33). Period = month running mean, * = $p < 0.05$, ** = $p < 0.01$, Sign = sign of regression coefficient.

		Driver 1				Driver 2				Driver 3			
Date	***Spartina* Class**	**Driver**	**Period**	**R^2**	**Sign**	**Driver**	**Period**	**R^2**	**Sign**	**Driver**	**Period**	**R^2**	**Sign**
(A) All Dates	Tall	MNT	3	0.271 **	+	TP	3	0.185 **	+	RD	9	0.158 **	+
	Medium	MNT	6	0.173 **	+	TP	3	0.153 **	+	RD	9	0.101 **	+
	Short	MNT	6	0.247 **	+	TP	3	0.137 **	+	PMSL	3	0.092 **	+
(B) Fall 2000–2011	Tall	FMSL	9	0.874 **	+	PDSI	0	0.802 **	+	SPI	0	0.751 **	+
	Medium	FMSL	9	0.840 **	+	TP	0	0.773 **	+	PDSI	0	0.766 **	+
	Short	PMSL	9	0.766 **	+	SPI	0	0.745 **	+	TP	0	0.646 **	+
(C) Fall	Tall	PDSI	3	0.324 **	+	MP	3	0.262 **	+	RD	6	0.241 **	+
	Medium	PDSI	0	0.241 **	+	MP	3	0.223 **	+	RD	6	0.185 **	+
	Short	MP	3	0.212 **	+	SPI	3	0.203 **	+	FMSL	6	0.197 **	−
(D) November–December	Tall	TP	3	0.313 **	+	PDSI	6	0.296 **	+	RD	6	0.279 **	+
	Medium	TP	3	0.379 **	+	PDSI	6	0.248 **	+	RD	6	0.239 **	+
	Short	TP	3	0.371 **	+	SPI	6	0.226 **	+	FMSL	6	0.183 **	−
(E) Januar–February	Tall	PMSL	3	0.256 **	+	MNT	9	0.197 **	+	SPI	6	0.156 **	+
	Medium	PMSL	3	0.242 **	+	MNT	9	0.230 **	+	RD	9	0.117*	+
	Short	MXT	9	0.261 **	+	PMSL	3	0.199 **	+	SPI	6	0.076	+
(F) April–May	Tall	RD	6	0.284 **	+	PDSI	3	0.155 **	+	SPI	6	0.144 **	+
	Medium	RD	3	0.292 **	+	PDSI	3	0.158 **	+	SPI	9	0.137 **	+
	Short	RD	6	0.180 **	+	TP	6	0.099 **	+	PDSI	3	0.089 **	+
(G) July-August	Tall	SPI	9	0.535 **	+	RD	9	0.411 **	+	PDSI	9	0.406 **	+
	Medium	SPI	9	0.452 **	+	RD	9	0.354 **	+	PDSI	9	0.323 **	+
	Short	SPI	9	0.349 **	+	TP	9	0.288 **	+	PDSI	9	0.238 **	+

References

1. Mitsch, W.J.; Gosselink, J.G. *Wetlands*; John Wiley and Sons: Hoboken, NJ, USA, 2007.
2. Barbier, E.B.; Hacker, S.D.; Kennedy, C.; Koch, E.W.; Stier, A.C.; Silliman, B.R. The value of estuarine and coastal ecosystem services. *Ecol. Monogr.* **2011**, *81*, 169–193. [CrossRef]
3. Gosselink, J.G.; Odum, E.P.; Pope, R.M. *The Value of the Tidal Marsh*; Center for Wetland Resources, Louisiana State University: Baton Rouge, LA, USA, 1974.
4. Day, J.W.; Christian, R.R.; Boesch, D.M.; Yáñez-Arancibia, A.; Morris, J.; Twilley, R.R.; Naylor, L.; Schaffner, L.; Stevenson, C. Consequences of climate change on the ecogeomorphology of coastal wetlands. *Estuaries Coasts* **2008**, *31*, 477–491. [CrossRef]
5. Simas, T.; Nunes, J.P.; Ferreira, J.G. Effects of global climate change on coastal salt marshes. *Ecol. Model.* **2001**, *139*, 1–15. [CrossRef]
6. Scavia, D.; Field, J.C.; Boesch, D.F.; Buddemeier, R.W.; Burkett, V.; Cayan, D.R.; Fogarty, M.; Harwell, M.A.; Howarth, R.W.; Mason, C.; *et al.* Climate change impacts on U.S. coastal and marine ecosystems. *Estuaries* **2002**, *149*, 149–164. [CrossRef]
7. Hoegh-Guldberg, O.; Bruno, J.F. The impact of climate change on the world's marine ecosystems. *Science* **2010**, *328*, 1523–1528. [CrossRef] [PubMed]
8. Bilskie, M.V.; Hagen, S.C.; Medeiros, S.C.; Passeri, D.L. Dynamics of sea level rise and coastal flooding on a changing landscape. *Geophys. Res. Lett.* **2014**, *41*, 927–934. [CrossRef]
9. Wu, X.; Liu, H. Consistent shifts in spring vegetation green-up date across temperate biomes in China, 1982–2006. *Glob. Chang. Biol.* **2013**, *19*, 870–880. [CrossRef] [PubMed]
10. Charles, H.; Dukes, J.S. Effects of warming and altered precipitation on plant and nutrient dynamics of a New England salt marsh. *Ecol. Appl.* **2009**, *19*, 1758–1773. [CrossRef] [PubMed]
11. Feagin, R.A.; Martinez, M.L.; Mendoza-Gonzalez, G.; Costanza, R. Salt marsh zonal migration and ecosystem service change in response to global sea level rise: A case study from an urban region. *Ecol. Soc.* **2010**, *15*, 14.
12. Osland, M.J.; Enwright, N.; Day, R.H.; Doyle, T.W. Winter climate change and coastal wetland foundation species: Salt marshes *vs.* mangrove forests in the southeastern United States. *Glob. Chang. Biol.* **2013**, *19*, 1482–1494. [CrossRef] [PubMed]
13. Throne, K.M.; Takekawa, J.Y.; Elliot-Fisk, D.L. Ecological effects of climate change on salt marsh wildlife: A case study from a highly urbanized estuary. *J. Coast. Res.* **2012**, *28*, 1477–1487. [CrossRef]
14. Patience, N.; Klemas, V. *Wetland Functional Health Assessment Using Remote Sensing and Other Techniques: Literature Search*; NOAA Technical Memorandum NMFS-SEFSC-319. National Technical Information Service: Springfield, VA, USA, 1993.
15. Klemas, V.V. Remote sensing of landscape-level coastal environmental indicators. *Environ. Manag.* **2001**, *27*, 47–57. [CrossRef] [PubMed]
16. Klemas, V. Remote sensing of coastal wetland biomass: An overview. *J. Coast. Res.* **2013**, *29*, 1016–1018. [CrossRef]
17. Mishra, D.R.; Cho, H.J.; Ghosh, S.; Fox, A.; Downs, C.; Merani, P.B.T.T.; Kirui, P.; Jackson, N.; Mishra, S. Post-spill state of the marsh: Remote estimation of the ecological impact of the Gulf of Mexico oil spill on Louisiana Salt Marshes. *Remote Sens. Environ.* **2012**, *118*, 176–185. [CrossRef]
18. Ghosh, S.; Mishra, D.R.; Gitelson, A.A. Long-term monitoring of biophysical characteristics of tidal wetlands in the northern Gulf of Mexico—A methodological approach using MODIS. *Remote Sens. Environ.* **2016**, *173*, 39–58. [CrossRef]
19. Rouse, J.W.; Haas, R.H.; Schell, J.A.; Deering, D.W. Monitoring vegetation systems in the Great Plains with ERTS. *Third Earth Resources Technology Satellite–1 Symposium*; Freden, S.C., Mercanti, E.P., Becker, M., Eds.; NASA: Washington, DC, USA, 1974; pp. 309–317.
20. Wieski, K.; Pennings, S.C. Climate Drivers of *Spartina alterniflora* saltmarsh production in Georgia, USA. *Ecosystems* **2014**, *17*, 473–484. [CrossRef]
21. Wiegert, R.G.; Pomeroy, L.R.; Wiebe, W.J. Ecology of salt marshes: An introduction. In *The Ecology of a Salt Marsh*; Pomeroy, L.R., Wiegert, R.G., Eds.; Springer-Verlag: New York, NY, USA, 1981; pp. 3–19.
22. Chalmers, A.G. *The Ecology of the Sapelo Island National Estuarine Research Reserve*; University of Georgia Marine Institute: Sapelo Island, GA, USA, 1997.

23. Sullivan, B. *Sapelo Island National Estuarine Research Reserve Management Plan. 2008–2013*; National Oceanic and Atmospheric Administration and Sapelo Island National Estuarine Research Reserve: Sapelo Island, GA, USA, 2008.
24. Hladik, C.; Schalles, J.; Alber, M. Salt marsh elevation and habitat mapping using hyperspectral and LIDAR data. *Remote Sens. Environ.* **2013**, *139*, 318–330. [CrossRef]
25. Pennings, S.C.; Bertness, M.D. Salt marsh communities. In *Marine Community Ecology*; Hay, M.E., Ed.; Sinauer Associates: Sunderland, UK, 2001; pp. 289–316.
26. Hladik, C.; Alber, M. Accuracy assessment and correction of a LIDAR-derived salt marsh digital elevation model. *Remote Sens. Environ.* **2012**, *121*, 224–235. [CrossRef]
27. Schalles, J.F.; Hladik, C.M.; Lynes, A.A.; Pennings, S.C. Landscape estimates of habitat types, plant biomass, and invertebrate densities in a Georgia salt marsh. *Oceanography* **2013**, *26*, 88–97. [CrossRef]
28. Kovalskyy, V.; Roy, D.P. The global availability of Landsat 5 TM and Landsat 7 ETM+ land surface observations and implications for global 30 em Landsat data product generation. *Remote Sens. Environ.* **2013**, *130*, 280–293. [CrossRef]
29. USGS Glovis Website. Available online: http://glovis.usgs.gov (accessed on 4 January 2013).
30. Landsat Processing Details. Available online: http://landsat.usgs.gov/Landsat_Processing_Details.php (accessed on 4 January 2013).
31. Lee, D.S.; Storey, J.C.; Choate, M.J.; Hayes, R.W. Four years of Landsat-7 On-Orbit geometric calibration and performance. *IEEE Trans. Geosci. Remote Sens.* **2004**, *42*, 2786–2795. [CrossRef]
32. Kearney, M.S.; Stutzer, D.; Turpie, K.; Stevenson, J.C. The effects of tidal inundation on the reflectance characteristics of coastal marsh vegetation. *J. Coast. Res.* **2009**, *256*, 1177–1186. [CrossRef]
33. O'Donnell, J.P.R.; Schalles, J.F. Development of a biomass algorithm for the marsh grass *Spartina alterniflora* Loisel using Landsat 5 Thematic Mapper satellite imagery. *Estuar. Coast.* **2016**. (in prepare).
34. Masek, J.G.; Vermote, E.F.; Saleous, N.E.; Wolfe, R.; Hall, F.G.; Huemmrich, K.F.; Gao, F.; Kutler, J.; Lim, T.K. A landsat surface reflectance dataset for North America, 1990–2000. *IEEE Geosci. Remote Sens. Lett.* **2006**, *3*, 68–72. [CrossRef]
35. Wu, H.; Li, Z.-L. Scale issues in remote sensing: A review on analysis, processing and modeling. *Sensors* **2009**, *9*, 1768–1793. [CrossRef] [PubMed]
36. Baccini, A.; Friedl, M.A.; Woodcock, C.E.; Zhu, Z. Scaling field data to calibrate and validate moderate spatial resolution remote sensing models. *Photogramm. Eng. Remote Sens.* **2007**, *73*, 945–954.
37. Gitelson, A.A. Wide dynamic range vegetation index for remote quantification of biophysical characteristics of vegetation. *J. Plant Physiol.* **2004**, *173*, 165–173. [CrossRef] [PubMed]
38. Gitelson, A.A.; Gritz, Y.; Merzlyak, M.N. Relationships between leaf chlorophyll content and spectral reflectance and algorithms for non-destructive chlorophyll assessment in higher plant leaves. *J. Plant Physiol.* **2003**, *160*, 271–282. [CrossRef] [PubMed]
39. USGS Water Data Website. Available online: http://waterdata.usgs.gov (accessed on 4 March 2014).
40. NOAA Tides and Currents Website. Available online: http://tidesandcurrents.noaa.gov (accessed on 4 March 2014).
41. NOAA National Centers for Environmental Information Website. Available online: http://ncdc.noaa.gov (accessed on 4 March 2014).
42. NOAA National Weather Service. Available online: http://www.weather.gov (accessed on 4 March 2014).
43. JMP Statistical Discovery. Available online: http://www.jmp.com (accessed on 4 March 2014).
44. O'Brien, R.M. A caution regarding rules of thumb for variance inflation factors. *Qual. Quant.* **2007**, *41*, 673–690. [CrossRef]
45. Reimold, R.J.; Gallagher, J.L.; Thompson, D.E. Remote sensing of tidal marsh. *Photogramm. Eng.* **1973**, *39*, 477–488.
46. Dai, T.; Wiegert, R.G. Ramet population dynamics and net aerial primary productivity of *Spartina alterniflora*. *Ecology* **1996**, *77*, 276–288. [CrossRef]
47. Morris, J.; Sundberg, K.; Rodriguez, D.; Hankinson, W.; Krest, R.L.; Haskin, B. Long-Term *Spartina. alterniflora* Biomass, Productivity, Porewater Chemistry and Marsh Elevation in North Inlet Estuary. Georgetown, SC: 1984–2015. Available online: http://links.baruch.sc.edu/data/accessfiles/North_Inlet_Long_Term_Spartina_alterniflora_database_1984_2015.zip (accessed on 27 May 2016).

48. Jung, Y.; Burd, A. Variability of non-structural carbohydrates in *Spartina alterniflora* measured in a Georgia saltmarsh. Available online: http://www.sgmeet.com/jasm2014/viewabstract.asp?AbstractID=13484 (accessed on 3 June 2016).
49. Gallagher, J.L.; Reimold, R.J.; Linthurst, R.A.; Pfeiffer, W.J. Aerial production, mortality, and mineral accumulation-export dynamics in *Spartina alterniflora* and *Juncus roemerianus* plant stands in a Georgia salt marsh. *Ecology* **1980**, *61*, 303. [CrossRef]
50. Odum, E.P.; Finn, J.T.; Franz, E.H. Perturbation theory and the subsidy-stress gradient. *Deep Sea Res. Part B Oceanogr. Lit. Rev.* **1979**, *26*, 811. [CrossRef]
51. Bertness, M.D.; Pennings, S.C. Spatial variation in process and pattern in salt marsh plant communities in eastern North America. In *Concepts and Controversies in Tidal Marsh Ecology*; Weinstein, M.P., Kreeger, D.A., Eds.; Kluwer Academic Publisher: Dordrecht, The Netherlands, 2000; pp. 39–57.
52. Mendelssohn, I.A.; Morris, J.T. Eco-physiological controls on the productivity of *Spartina alterniflora* Loisel. In *Concepts and Controversies in Tidal Marsh Ecology*; Weinstein, M.P., Kreeger, D.A., Eds.; Kluwer Academic Publisher: Dordrecht, The Netherlands, 2000; pp. 59–80.
53. Silliman, B.R.; van de Koppel, J.; Bertness, M.D.; Stanton, L.E.; Mendelssohn, I.A. Drought, snails, and large-scale die-off of Southern U.S. salt marshes. *Science* **2005**, *310*, 1803–1806. [CrossRef] [PubMed]
54. Dame, R.; Kenny, P. Variability of *Spartina alterniflora* primary production in the euhaline North Inlet estuary. *Mar. Ecol. Prog. Ser.* **1986**, *32*, 71–80. [CrossRef]
55. Gross, M.F.; Hardisky, M.A.; Klemas, V. Inter-annual spatial variability in the response of *Spartina alterniflora* biomass to amount of precipitation. *Photogramm. Eng. Remote Sens.* **1990**, *6*, 949–960.
56. Di Iorio, D.; Castelao, C.M. The dynamical response of salinity to freshwater discharge and wind forcing in adjacent estuaries on the Georiga Coast. *Oceanography* **2013**, *26*, 44–51. [CrossRef]
57. Weston, N.B.; Hollibaugh, J.; Sandow, J.; Joye, S. Nutrients and dissolved organic matter in the Altamaha River and loading to coastal zone. In *Georgia Water Resource Conference*; Hatcher, K.J., Ed.; Institute of Ecology, University of Georgia: Athens, GA, USA, 2003.
58. Morris, J.T.; Sundberg, K.; Hopkinson, C.S. Salt marsh primary production and its response to relative sea level and nutrients in estuaries at Plum Island, Massachusets, and North Inlet, South Carolina, USA. *Oceanography* **2013**, *26*, 78–84. [CrossRef]
59. Giurgevich, J.R.; Dunn, E.L. Patterns of CO_2 and water vapor exchange of the tall and short height forms of *Spartina alterniflora* Loisel in a Georgia salt marsh. *Oecologia* **1979**, *43*, 139–156. [CrossRef]
60. Kirwan, M.L.; Guntenspergen, G.R.; Morris, J.T. Latitudinal trends in *Spartina alterniflora* productivity and the response of coastal marshes to global change. *Glob. Chang. Biol.* **2009**, *15*, 1982–1989. [CrossRef]
61. Elmer, W.H.; Useman, S.; Schneider, R.W.; Marra, R.E.; LaMondia, J.A.; Mendelssohn, I.A.; Jiménez-Gasco, M.M.; Caruso, F.L. Sudden vegetation dieback in Atlantic and Gulf Coast salt marshes. *Plant Dis.* **2013**, *97*, 436–445. [CrossRef]
62. Alber, M.; Swenson, E.M.; Adamowicz, S.C.; Mendelssohn, I.A. Salt marsh dieback: An overview of recent events in the US. *Estuar. Coast. Shelf Sci.* **2008**, *80*, 1–11. [CrossRef]
63. Silliman, B.R.; Zieman, J.C. Top-down control of *Spartina alterniflora* production by periwinkle grazing in a Virginia salt marsh. *Ecology* **2001**, *82*, 2830. [CrossRef]
64. Allen, C.D.; Breshears, D.D.; McDowell, N.G. On underestimation of global vulnerability to tree mortality and forest die-off from hotter drought in the Anthropocene. *Ecosphere* **2015**, *6*, 129. [CrossRef]
65. Wilson, C.A.; Hughes, Z.J.; FitzGerald, D.M. The effects of crab bioturbation on Mid-Atlantic saltmarsh tidal creek extension: Geotechnical and geochemical changes. *Estuar. Coast. Shelf Sci.* **2012**, *106*, 33–44. [CrossRef]